The Astrophysical Journal, 697:452–457, 2009 May 20 doi:10.1088/0004-637X/697/1/452

AKARI NEAR- AND MID-INFRARED SPECTROSCOPY OF APM 08279+5255 AT $z = 3.91$*

S. Oyabu[1], K. Kawara[2], Y. Tsuzuki[3], Y. Matsuoka[2,5,6], H. Sameshima[2], N. Asami[2], and Y. Ohyama[4]
[1] Institute of Space and Astronautical Science, Japan Aerospace Exploration Agency, 3-1-1 Yosinodai, Sagamihara, Kanagawa 229-8510, Japan; oyabu@ir.isas.jaxa.jp
[2] Institute of Astronomy, University of Tokyo, 2-21-1 Osawa, Mitaka, Tokyo 181-0015, Japan
[3] System Integration Service Department, Redfox Inc., 3-3-11, Kita-Aoyama, Minato-ku, Tokyo 107-0061, Japan
[4] Academia Sinica, Institute of Astronomy and Astrophysics, Taiwan
Received 2008 July 4; accepted 2009 March 16; published 2009 May 1

ABSTRACT

We present rest-frame optical/near-infrared spectra of the gravitationally lensed quasar APM 08279+5255 at $z = 3.91$ that has been taken using the Infrared Camera (IRC) onboard the *AKARI* infrared satellite. The observed continuum consists of two components; a power-law component dominating optical wavelengths which is the direct light from the central source and thermal emission dominating near-infrared wavelengths which is attributed to the emission from hot dust in the circumnuclear region. The thermal emission well represents optically thick emission by hot dust at $T \sim 1300$ K with $\tau_{2\,\mu m} > 2$ and apparent mass, $M_{hot} > 10\ M_{\odot}$. Thus, our observations directly detected the optically thick region of hot dust in APM 08279+5255. H I recombination lines of Hα (0.656 μm), Paα (1.875 μm), and Paβ (1.282 μm) are clearly detected at 3.2, 6.3, and 9.3 μm. Simulations with the photoionization models suggest that APM 08279+5255 has broad-line region (BLR) clouds characterized by $\log n_H \sim 12$–14 for the gas density, $\log U \sim -2$ to -6 for the ionization parameter, and $E(B-V) \sim 0.3$–0.6 for the BLR. Thus, optically thick emission of hot dust supports an idea on nonspherical distribution of dust near the central source, consistent with the active galactic nuclei model with the dust torus. The temperature of hot dust and flux ratios of these H I lines are similar to those observed in low-redshift quasars. There are significant time variations in the H I lines, which are probably caused by variations in the brightness of the central source.

Key words: galaxies: active – infrared: galaxies – quasars: emission lines – quasars: general – quasars: individual (APM 08279+5255)

1. INTRODUCTION

High-redshift quasars provide direct probes of the distant early universe where galaxies and quasars formed. Over the past decade, many high-redshift quasars have been found in large-area surveys such as the Sloan Digital Sky Survey (York et al. 2000) and Two Degree Field (2dF) QSO Redshift Survey (Boyle et al. 2000). Nonetheless, no convincing evidences for evolution in quasar spectra have been found, which is in remarked contrast to spectra of galaxies. For example, the flux ratio Fe II/Mg II in quasars is expected to be small at high redshift because the Fe-enrichment is delayed relative to the α-element enrichment (i.e., Yoshii et al. 1998). However, Fe II/Mg II does not change from low-redshift to high-redshift (Wills et al. 1985; Tsuzuki et al. 2006; Kawara et al. 1996; Iwamuro et al. 2004; Kurk et al. 2007; Barth et al. 2003). Other UV emission lines such as N V and C IV show no evidence for evolution either (Dietrich et al. 2003; Nagao et al. 2006).

Dust locating at the circumnuclear region is heated by the central engine, and produce near-infrared radiation. Such hot dust is common in active galactic nuclei (AGNs) and quasars at low redshift and also observed in high-redshift quasars (Oyabu et al. 2001; Hines et al. 2006; Jiang et al. 2006). Dust at high redshift is presumably produced as a result of supernova explosions, while dust production would be dominated by mass loss of late-type stars at low redshift. If so, hot dust at high redshift would be different from that at low redshift. Unfortunately, hot dust in the high redshift has been mostly studied based on broadband photometry (Oyabu et al. 2001; Hines et al. 2006; Jiang et al. 2006), and no systematic evolution has been reported. Spectroscopic studies would provide new insight into evolution and origin of hot dust in the circumnuclear region of quasars.

AKARI, which was launched in 2006 February, is the first Japanese satellite dedicated to infrared observations (Murakami et al. 2007). It has a 68.5 cm diameter telescope LHe-cooled to 5.4 K. In addition to its major mission that is to perform all-sky survey at six bands in the mid- and far-infrared, *AKARI* has carried out pointed observations for deep surveys of selected area and systematic observations of important objects.

We have performed the near- and mid-infrared spectroscopy of the quasar APM 08279+5255 at $z = 3.91$ using Infrared Camera (IRC; Onaka et al. 2007) onboard *AKARI*. These observations were obtained as part of *AKARI* Open Time program "IRC NIR Spectroscopy of High-Redshift Quasars."

APM 08279+5255 was discovered during a survey for high Galactic latitude carbon stars (Irwin et al. 1998). The IR flux densities at 25, 60, and 100 μm are 0.23, 0.51, and 0.95 Jy, respectively, in the *IRAS* Faint Source Catalog (Moshir et al. 1992). This is apparently one of the most luminous objects with $5 \times 10^{15}\ L_{\odot}$ at $z = 3.91$ (Downes et al. 1999). The ground-based imagery observations in the optical (Ibata et al. 1999) and near- and mid-infrared (Egami et al. 2000), revealed that APM 08279+5255 is gravitationally lensed with a magnification of ~100. Using the Infrared Spectrograph on the *Spitzer Space Telescope*, Soifer et al. (2004) detected broad Paα and Paβ H I recombination lines as well as a strong, red continuum in the rest-frame wavelength range 1–7 μm.

Throughout this paper, $\Omega = 0.3$, $\Lambda = 0.7$, and $h = 0.7$ are assumed for cosmology parameters.

* Based on observations with *AKARI*, a JAXA project with the participation of ESA.
[5] Research Fellow of the Japan Society for the Promotion of Science.
[6] Present address: Graduate School of Science, Nagoya University, Furo-cho, Chikusa-ku, Nagoya 464-8602, Japan.

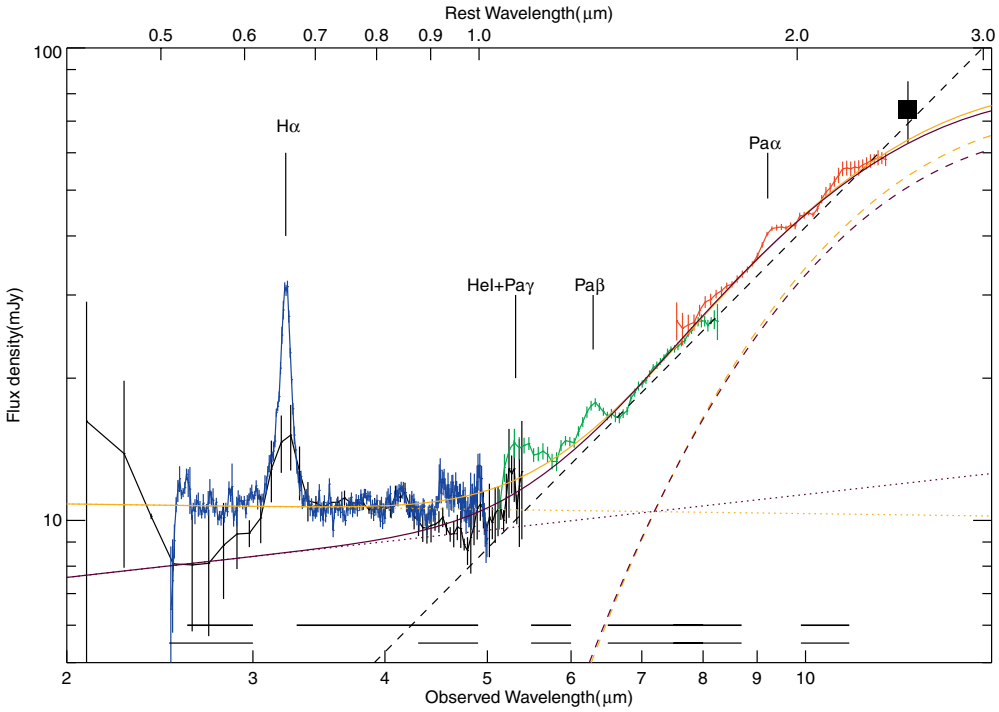

Figure 1. NP (black line), NG (blue), SG1 (green), and SG2 (red) spectra of APM 08279+5255, plotted as flux density vs. wavelength (observed, bottom scale; rest frame, top-scale). The vertical lines indicate the measurement error. A power-law fit, $f_\nu \sim \nu^{-2.26}$, to the continuum for $\lambda_{\rm obs} < 15$ μm, which is derived from the *Spitzer* IRS observation, is shown as a black dashed line (Soifer et al. 2004). The filled square presents the 12.5 μm flux density measured by Egami et al. (2000). Two combined fits shown in orange and purple solid lines indicate two kinds of fits: an orange one used NG data for NIR data and a purple fitted a dip around 2.3–3 μm on NP data corresponding to an extreme case. The power-law components are shown in orange and purple dotted lines, and the blackbodies shown in dashed lines with the same colors. The black lines at the bottom mark the places used in the continuum fitting. The upper thick ones are used for the case of NG and the others are for NP data with a dip.

Table 1
Observational Log and Modes (AOT04)

Obs. Date (UT)	Pointing ID	Channel/Disperser	Wavelength (μm)	Resolving Power	Extraction Aperture
2006 Oct 19	3120025.001	NIR/NP	1.8–5.5	19 at 3.5 μm	7.″5
		MIR-S/SG1	4.6–9.2	53 at 6.6 μm	12.″5
		MIR-S/SG2	7.2–13.4	50 at 10.6 μm	12.″5
2007 Apr 16	3120050.001	NIR/NG	2.5–5.0	120 at 3.6 μm	7.″5

2. OBSERVATION AND DATA REDUCTION

Spectroscopy was performed on APM 08279+5255 using the IRC (Onaka et al. 2007; Ohyama et al. 2007) onboard the *AKARI* satellite (Murakami et al. 2007) on 2006 October and 2007 April. The observations are summarized in Table 1.

We used two IRC's channels, NIR and MIR-S. Each covers different wavelengths from the near-infrared to mid-infrared. The NIR channel uses a 512 × 412 InSb array, whereas the MIR-S employs a 256 × 256 Si:As array. The NIR and MIR-S channels share the same field of views and observe simultaneously.

The Astronomical Observational Template 04 (AOT04) designed for spectroscopy was used. AOT04 replaces the imaging filters by transmission-type dispersers on the filter wheels to take near- and mid-infrared spectra. For 2006 October observations, the NIR Prism (NP) was set to cover the wavelength of 1.8–5.5 μm with a spectral resolving power of $R \sim$19 at 3.5 μm. The target was put on the center of the detector array without a slit. In the MIR-S channel, two grisms, SG1 (4.6–9.2 μm; $R \sim 53$) and SG2 (7.2–13.4 μm; $R \sim 50$), were set and slitless spectroscopy was made. For 2007 April observations, the NIR grism (NG) was set to cover the wavelength of 2.5–5 μm with the resolution $R \sim 120$. The $1' \times 1'$ slit was used to avoid the confusion of spectra.

The data were processed through the IRC-dedicated data reduction package, IRC_SPECRED version 20080528 (Ohyama et al. 2007). First, dark subtraction, linearity correction, flat correction, and various image anomaly corrections were performed. Multiple exposures were then co-added. After performing wavelength- and flux-scaling, the spectra of the object were extracted. Apertures for the spectrum extraction were 5 pixels, namely, (NP, SG1, SG2, NG) = (7.″5, 12.″5, 12.″5, 7.″5). Aperture correction was also performed at the end.

We found large uncertainties associated with the SG1 and SG2 calibration at $\lambda_{\rm obs} > 8.3$ μm and $\lambda_{\rm obs} > 12.0$ μm, respectively. This was caused by the second-order light affecting the response curves of both grisms. Thus, in this work, we only use the wavelength at $\lambda_{\rm obs} < 8.3$ μm and $\lambda_{\rm obs} < 12.0$ μm for the SG1 and SG2 spectra, respectively.

3. RESULTS

Figure 1 shows the spectra of APM 08279+5255 in the NP, NG, SG1, and SG2 bands. The continuum and emission lines are clearly detected at 2–13 μm.

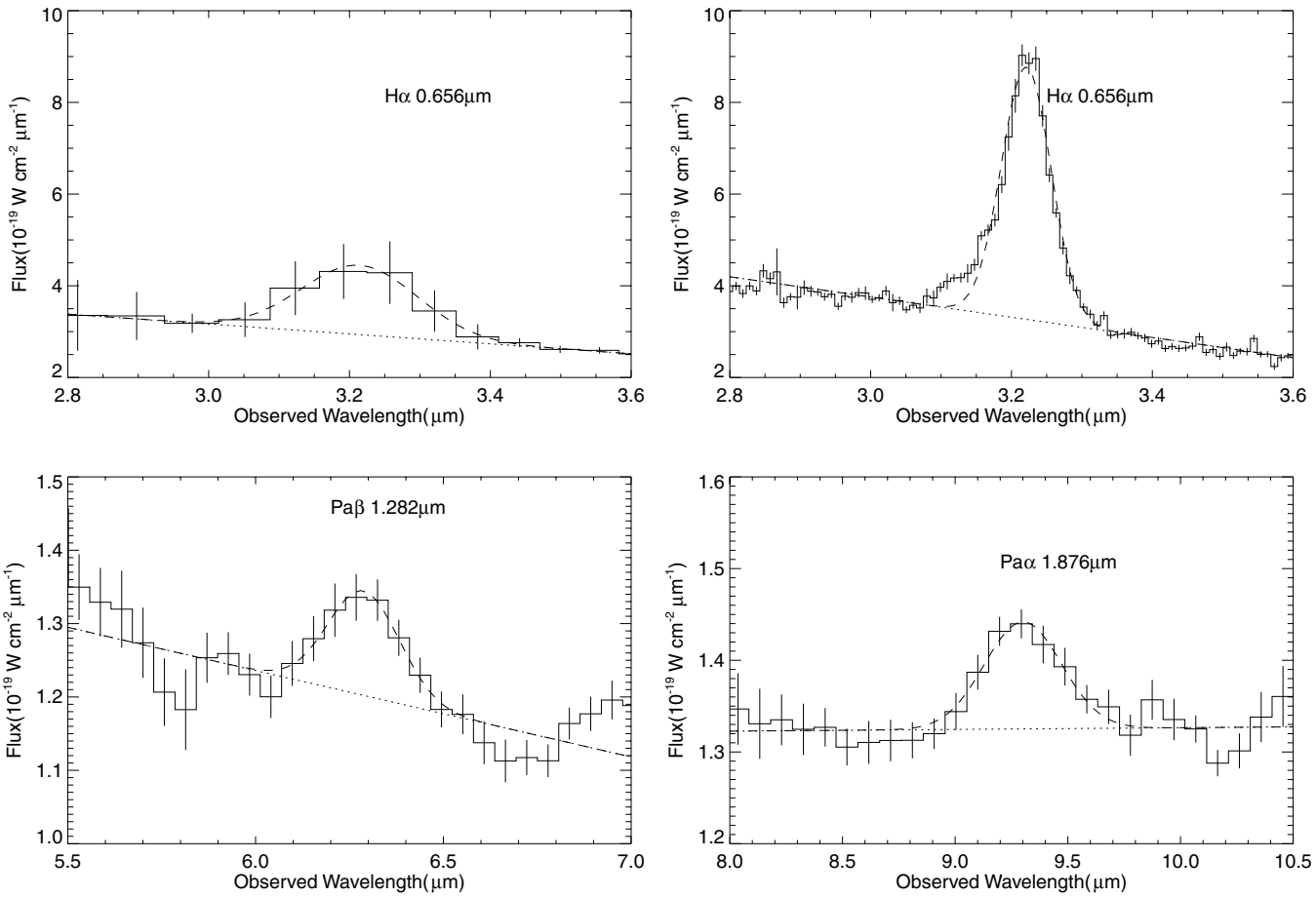

Figure 2. Profiles of emission lines: (top left) Hα on NP, (top right) Hα on NG, (bottom left) Paβ on SG1, and (bottom right) Paβ on SG2. The histograms are from *AKARI* data. The vertical lines represent their errors. The dotted and dashed lines show the fitted continuum and an emission line, respectively.

The continuum shows two components; one is a flat power law at $\lambda_{\rm rest} \lesssim 1$ μm, whereas the other is a power law or bump sharply rising beyond $\lambda_{\rm rest} \gtrsim 1$ μm, where $\lambda_{\rm rest}$ denotes rest-frame wavelengths. Assuming the models consisting of two power-law components, the best fit to the data is $f_\nu \sim \nu^{0.03}$ for $\lambda_{\rm rest} < 1$ μm and $f_\nu \sim \nu^{-2.23}$ for $\lambda_{\rm rest} > 1$ μm. The overall continuum level and the power-law slope for $\lambda_{\rm rest} > 1$ μm is consistent with observations of *Spitzer* IRS spectroscopy (Soifer et al. 2004).

H I recombination lines of Hα (0.656 μm), Paα (1.875 μm), and Paβ (1.282 μm) are clearly detected at 3.21, 6.3, and 9.3 μm. The He I $2^3S - 2^3P$ (1.083 μm) line and H I Paγ (1.094 μm) line are blended and seen as a bump at 5.4 μm.[7] The line fluxes are measured, as illustrated in Figure 2, by fitting a linear function to the local continuum data on either side of the line profile, and then fitting a Gaussian function to the linear-function-subtracted spectrum. The results including line fluxes and FWHMs are summarized in Table 2. At the bottom of this table, the data obtained by the *Spitzer* (Soifer et al. 2004) are given to facilitate the comparison. The *Spitzer* strengths of Paα and Paβ are significantly greater than those obtained with *AKARI* by a factor of 1.5–2. This will be discussed later.

This is the first Hα detection in APM 08279+5255. The Hα fluxes in APM 08279+5255 are 60–100 times brighter than that in RX J1759.4+6638, a quasar at similar redshift, $z = 4.3$ (Oyabu et al. 2007). However, the line flux of Hα is similar between them, consistent with the lens magnification of ∼100.

While the continuum fluxes observed on two occasions in a six month interval are consistent with each other, the Hα fluxes varied at a 2.3σ level from the first occasion to the other. The Hα flux measured with NP on the first occasion is $F(\mathrm{H}\alpha) = (313 \pm 84) \times 10^{-22}$ W cm^{-2}, while the second measurement with NG gives $F(\mathrm{H}\alpha) = (509 \pm 7) \times 10^{-22}$ W cm^{-2}. Although the different dispersers were used, we believe that this variation is real. In fact, as compared in Table 2, the Paβ and Paα strengths observed with *Spitzer* differ by a factor of 1.5–2 from those observed with *AKARI* three years later. On the other hand, no significant variations in continuum have been observed between *Spitzer* and *AKARI* observations. This will be discussed again in Section 4.3.

4. DISCUSSION

4.1. Hot Dust in a $z = 3.9$ Quasar

The spectral energy distribution (SED) of quasars can be modeled with two components, big blue and infrared bumps (Sanders et al. 1989; Elvis et al. 1994). A big blue bump has been considered to be direct light from the central engine, while the infrared bump is attributed to thermal emission by dust which absorbs UV/optical light and re-emit it in the infrared. The sharp rise from $\lambda_{\rm rest} \sim 1$ μm toward the peak of the infrared bump is especially attributed to hot dust surrounding the central source. We assumed that the observed spectra only consist of a

[7] Models consisting of two lines poorly fit to the data; the O I λ11287 μm emission line might contribute to the bump.

Table 2
Line Flux Measurements of APM 08279+5255

Channel/ Disperser	Line	Obs. Wavelength (μm)	Redshift	FWHM (km s^{-1})	Obs. Flux (10^{-22} W cm^{-2})	Obs. EW[a] (μm)
Observation on 2006 Oct 19						
NIR/NP	Hα 0.656 μm	3.21 ± 0.04	3.90 ± 0.06	<18300	313 ± 84	0.107 ± 0.029
MIR-S/SG1	Paβ 1.282 μm	6.28 ± 0.03	3.90 ± 0.02	<12300	42 ± 6	0.036 ± 0.005
MIR-S/SG2	Paα 1.875 μm	9.30 ± 0.05	3.96 ± 0.02	<13800	57 ± 6	0.043 ± 0.005
Observation on 2007 Apr 16						
NIR/NG	Hα 0.656 μm	3.22 ± 0.01	3.91 ± 0.02	7721	509 ± 7	0.159 ± 0.002
Spitzer IRS Observation on 2003 Nov 23 (Soifer et al. 2004)						
	Paβ 1.282 μm	6.315 ± 0.013	3.925 ± 0.006	9500	81 ± 16	0.061
	Paα 1.875 μm	9.235 ± 0.011	3.914 ± 0.011	8770	85 ± 11	0.059

Note. [a] The observed equivalent width (EW) of emission lines.

power-law emission and a single-temperature blackbody, representing the big blue bump and the infrared bump, respectively. These models are defined as

$$F_\nu = C_1 \nu^\alpha + C_2 B_\nu(T_{\rm dust})(1 - {\rm e}^{-\tau_\nu}), \quad (1)$$

where α is a power-law index, $B_\nu(T_{\rm dust})$ is the Planck function with dust temperature $T_{\rm dust}$, and τ_ν is the dust optical depth. For the frequency dependence of the dust optical depth we adopt the result of Weingartner & Draine (2001).

The parameters, C_1, α, C_2, $T_{\rm dust}$, and τ_ν are derived by χ^2 fitting to the observed continuum. Near-infrared part of the spectrum was taken with NP and NG, resulting in two sets of the spectra, namely, NP-SG1-SG2 and NG-SG1-SG2. Fits to these two spectra resulted in the allowable temperature in 1σ error, 1270 K $< {\rm T_{dust}} <$ 1295 K, with $\alpha = -0.02 \pm 0.03$ for NP and 1250 K $< {\rm T_{dust}} <$ 1295 K with $\alpha = 0.03 \pm 0.03$ for NG. In the both case, the dust optical depths were just determined to be the lower limit, $\tau_{2\,\mu{\rm m}} \gtrsim 2$, which means that the hot dust emission of APM 08279+5255 is optically thick at a rest wavelength $\lesssim 2$ μm. Our observations directly detected the optically thick region of hot dust in the quasar. These fits were made to the continua after removing significant emission features from the observed spectra. If the broad deep dip at 2.5 μm of the NP spectrum is real continuum, as an extreme case to check the dependency of the dust temperature on the power-law index, $\alpha = -0.25$, $T_{\rm dust} = 1290$ K, and $\tau_{2\,\mu{\rm m}} \gtrsim 2$ are obtained. Thus, the dust temperature is 1280 $\pm$20 K.

Temperatures $\sim$1300 K of this quasar suggest that graphite and silicate grains can survive as the hot dust component in this quasar because sublimation temperatures for graphite and silicate grains are $T \sim 1800$ K and $\sim$1500 K, respectively (Salpeter 1977; Huffman 1977). We interpret the existence of such hot dust whose temperature is close to sublimation temperatures of dust as the innermost dust component heated by the strong radiation of the AGN central engine. The dust closer to the central engine has higher temperatures but cannot survive inside any critical radius at which it begins to sublimate.

As we fit the hot dust emission using a single-temperature blackbody of $\sim$1300 K in Figure 1, the luminosity of the hot dust is calculated at $L_{\rm hot} = 2.1 \times 10^{15}\ m^{-1}\ L_\odot$, where m is the magnification factor of the gravitational lensing. If it is assumed that the blackbody emission is due to heated dust grains, a measurement of the size of emitting region can be determined from the relationship,

$$F_\nu = m \frac{(1 - e^{-\tau_\nu}) B_\nu(T_{\rm dust})}{(1+z)^3} \pi \left(\frac{R_{\rm d}}{D_{\rm A}}\right)^2. \quad (2)$$

Here, F_ν is the observed flux density, m is the magnification factor, τ_ν is the optical depth, D_A is the angular diameter distance, and $R_{\rm d}$ is the radius of the emitting region. On the condition of $T_d \sim 1300$ K and optical thickness, $\tau_{2\,\mu{\rm m}} \gtrsim 2$, as derived above, the radius of emitting region is $R_{\rm d} = 10 m^{-1/2}$ pc. The size of the emitting region is small enough to magnify the flux of hot dust $\sim$100 times (Egami et al. 2000).

To measure the dust mass, $M_{\rm hot}$, which emit in the near-infrared, we used the following equation:

$$M_{\rm hot} = \frac{\tau_\nu}{k_d}\ \pi\ R_{\rm d}^2, \quad (3)$$

where k_d is the mass absorption coefficient according to Weingartner & Draine (2001). Now our fitting result is the optically thick condition, $\tau_{2\,\mu{\rm m}} > 2$, and thus we can obtain the lower limit of the dust mass, $M_{\rm hot} > 20\ m^{-1}\ M_\odot$ using 2 μm flux in the rest frame. We emphasize that the hot dust mass is much less than $7.5 \times 10^8\ m^{-1}\ M_\odot$ from warm dust with $T_{\rm dust} \sim 215$ K and $2.6 \times 10^9\ m^{-1}\ M_\odot$ from cold one with $T_{\rm dust} \sim 65$ K in Weiß et al. (2007), in which the continuum fluxes measured in the centimeter and millimeter are fit with the two-component dust model and their masses are calculated.

As studies of hot dust in low-redshift quasars, Kobayashi et al. (1993) observed low-resolution near-infrared spectra of 14 quasars with redshift $z < 0.3$ and reproduced their continua from 0.95 to 2.5 μm with a combination of two radiation components; the power law and blackbody of 1470 $\pm$ 90 K. There is also a recent work that Glikman et al. (2006) constructed the composite spectrum from 0.58 to 3.5 μm from near-infrared observations of 27 quasars with the redshift of $0.118 < z < 0.418$. Their composite spectrum is fitted with a spectral slope of -0.92 and a blackbody temperature of 1260 K. The dust temperature of APM 08279+5255 does not show a big difference from those of low-redshift quasars.

4.2. Hydrogen Recombination Lines

Our Paα/Paβ is 1.36 ± 0.24 in APM 08279+5255, which agrees with 1.05 ± 0.25 observed by Soifer et al. (2004). Landt et al. (2008) reported Paα/Paβ of 1.27 ± 0.07 for 16 low-redshift quasars. It should be noted that Paα/Paβ of

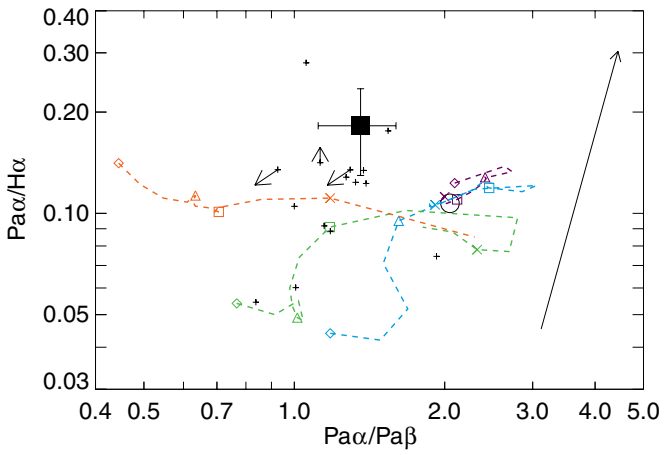

Figure 3. Paα/Paβ line flux ratio vs. the Paα/Hα ratio of APM 08279+5255 (large filled square calculated with Hα flux for NP). An open circle represents Case B values with $T = 10^4$ K and $n_{\rm H} = 10^4$ cm^{-3} (Osterbrock 1989). The small crosses represent the values of low-redshift quasars (Landt et al. 2008). The red, green, blue, and purple dashed lines show $\log n_{\rm H} = 14$, 12, 10, and 8, respectively. The diamond, triangle, square, and cross marks show $\log U = 0, -2, -4$, and -6. Details of the models is in the text. An arrow extends out along the reddening line to $E(B-V) = 1$.

0.64 ± 0.01 was obtained from a composite spectrum of low-redshift quasars (Glikman et al. 2006). In any case, Paα/Paβ observed in quasars is significantly smaller than 2.0 predicted from Case B recombination (Osterbrock 1989), suggesting that H I recombination lines come from broad-line region (BLR) clouds where the gas density is very high.

Figure 3 plots Paα/Paβ versus Paα/Hα of APM 08279+5255 along with low-redshift quasars(Landt et al. 2008). The APM 08279+5255 data used in this figure were taken in 2006 October when the three lines were observed simultaneously. Photoionization codes Cloudy (ver. 06.02 by Ferland et al. 1998) was used to probe BLR clouds. Our models for BLR clouds and the incident continuum from the central sources are the same as those used in Tsuzuki et al. (2006) and Matsuoka et al. (2007, 2008). The incident continuum is defined as

$$f_\nu \propto \nu^{\alpha_{\rm UV}} \exp(-h\nu/kT_{\rm CUT}) \exp(-kT_{\rm IR}/h\nu) + a\nu^{\alpha_{\rm X}}, \quad (4)$$

where $T_{\rm CUT}$ and $T_{\rm IR}$ is the high-energy and low-energy cutoff temperature, respectively. The low-energy cutoff temperature has little effect on the spectral result, thus a temperature $kT_{\rm IR} = 0.01$ Ryd is preset for the UV bump cutoff in the infrared. The UV and X-ray continuum components are combined using a UV to X-ray logarithmic spectra slope $\alpha_{\rm OX}$. We adopted a parameter set of $[T_{\rm CUT}, \alpha_{\rm UV}, \alpha_{\rm X}, \alpha_{\rm OX} = 1.5 \times 10^5$ K, $-0.2, -1.8, -1.4]$. The gas was modeled to have a constant hydrogen density $n_{\rm H}$ and exposed to the ionizing continuum radiation expressed with an ionization parameter U. We performed the calculation with the $(n_{\rm H}, U)$ sets in a range of 10^8 cm$^{-3} \leqslant {\rm n_H} \leqslant 10^{14}$ cm^{-3} and $10^{-7} \leqslant U \leqslant 10^0$ stepped by 0.5 dex.

As can see in Figure 3, none of the quasars agree with Case B recombination, regardless of intrinsic reddening to BLR clouds. The APM 08279+5255 data are reasonably represented with a parameter set of $\log n_{\rm H} \sim 12$–14 and $\log U \sim -2$ to -6 with $E(B-V) \sim 0.3$–0.6. Though optically thick region of hot dust surrounds the BLR, the intrinsic extinction in the BLR is moderate. This supports an idea of nonspherical distribution of hot dust near the central source, which is consistent with the AGN model with the dust torus (Antonucci & Miller 1985).

4.3. Variability of H I Recombination Lines

As discussed in Section 3, the line fluxes of Paα and Paβ have decreased by a factor of 1.5–2 in three years. In addition, the Hα flux also varied in six months. On the other hand, our continuum level of dust emission in $\lambda_{\rm rest} \gtrsim 1$ μm was kept constant over these periods. This means that the brightness in the BLR varied while that in thermal emission from hot dust was constant.

The variability of the broad lines and the constancy of the dust continuum can be explained in terms of the source size of the BLR and the hot dust emitting regions. For example, the size of the BLR of NGC 4151 is a few to 10 light days (i.e., Clavel et al. 1990; Maoz et al. 1991; Kaspi et al. 1996), while the inner boundary of the dusty torus extends to 48 light days from the central source (Minezaki et al. 2004). In the central source, the gas in the accretion disk, which is falling to the supermassive black hole, radiates the continuum from the high energy to the optical. Part of this continuum is absorbed in BLR clouds and thus ionized gas produces line emission such as H I recombination lines.

The incident continuum is also absorbed by dust which mainly exist at a distance greater than BLR clouds from the center. When the brightness of the incident continuum varies, BLR lines vary in a time delay of days or months and the thermal emission in the near- and mid-infrared radiation also varies after the time delay of months or years. Thus, the variation in the near- and mid-infrared radiation is smeared out more than that in recombination lines in BLR gas, making more difficult to detect variations in emission from hot dust than recombination lines.

It is unlikely that the variation in the H I recombination lines is attributed to microlensing events which have been observed lensed quasars (Burud et al. 2000, 2002; Hjorth et al. 2002; Jakobsson et al. 2005). The lensing galaxy of APM 08279+5255 has not been found. If the lensing galaxy is at $z = 1$–3, the Einstein radius of a star with 1 $M_\odot$ in the lensing galaxy is $\theta_{\rm E} \sim 1 \times 10^{-6}$ arcsec, or 7×10^{-3} at $z = 3.91$. This is much smaller than the size of hot dust which emits in the infrared, $10\ m^{-1/2}$ pc. Therefore, the microlensing event of a star in the lensing galaxy is unable to magnify infrared emission, while it is able to magnify fluxes coming from smaller regions like BLR clouds or an accretion disk. However, assuming the star in the lensing galaxy having a velocity of 300 km s^{-1}, the timescale of ∼30–100 years is longer than that of our detection of the variability (Chiba et al. 2005). Therefore, it might be difficult to explain that the variability is caused by microlensing.

5. SUMMARY

This paper presents near- and mid-infrared spectra of a gravitationally lensed quasar APM 08279+5255 at $z = 3.91$ with *AKARI*/IRC. The observations were performed with the IRC onboard the *AKARI* infrared satellite. We have detected the continuum from 2 μm to 13 μm in the observed frame, corresponding to 0.5–2.4 μm in the rest frame, and hydrogen emission lines of Hα, Paβ, and Paα and probably He I emission line. The major conclusions are as follows.

1. The thermal emission of hot dust heated by the central engine of this quasar is measured by the spectral fitting with the simple model expressed with a power-law and a blackbody. The thermal emission represents optically thick emission by hot dust at $T \sim 1300$ K with $\tau_{2\,\mu{\rm m}} > 2$ and mass, $M_{\rm hot} > 20\ m^{-1}\ M_\odot$. The temperature is consistent with those of low-redshift quasars which were

also measured spectroscopically (Kobayashi et al. 1993; Glikman et al. 2006).

2. The flux ratios of hydrogen emission lines, Hα, Paβ, and Paα, cannot be explained with the simple Case B recombination model, but they are consistent with those of low-redshift sample (Landt et al. 2008). Compared with the photoionization model, the physical condition of BLR in this quasar has a parameter set of $\log n_{\rm H} \sim 12$–14 and $\log U \sim -2$ to -6 with $E(B-V) \sim 0.3$–0.6. The moderate extinction in the BLR and optically thick emission of hot dust support an idea of nonspherical distribution of dust near the central source, consistent with the AGN model with the dust torus.
3. The difference between *AKARI* and *Spitzer* measurements in Paβ and Paα emission lines could be explained by the variability of this quasar. The variability of the Hα emission line was also detected with multiple observations with *AKARI* in a span of six months. There are two possibilities of variability for this quasars: the intrinsic variability of this quasar itself and the microlensing caused by a star in a lensing galaxy. Considering the timescale of microlensing, it might be ruled out for an explanation of the variability.

Our *AKARI* spectroscopic observations revealed that APM 08279+5255 at $z = 3.91$ shows a lack of evolution in the BLR and the hot dust component. This suggests that these components in this quasar have reached maturity very early on. This conclusion is probably applicable to most of the quasars because the studies of broad emission lines in high-redshift quasars show the lack of the evolution (i.e., Iwamuro et al. 2004) and the infrared photometric studies (Hines et al. 2006; Jiang et al. 2006) of quasars in $4.5 < z < 6.4$ do not differ significantly from those in low redshift.

AKARI is a JAXA project with the participation of ESA. We thank all the members of the *AKARI* project for their continuous help and support. We thank an anonymous referee for his or her suggestions.

REFERENCES

Antonucci, R. R. J., & Miller, J. S. 1985, ApJ, 297, 621
Barth, A. J., Martini, P., Nelson, C. H., & Ho, L. C. 2003, ApJ, 594, L95
Boyle, B. J., Shanks, T., Croom, S. M., Smith, R. J., Miller, L., Loaring, N., & Heymans, C. 2000, MNRAS, 317, 1014
Burud, I., et al. 2000, ApJ, 544, 117
Burud, I., et al. 2002, A&A, 391, 481
Chiba, M., Minezaki, T., Kashikawa, N., Kataza, H., & Inoue, K. T. 2005, ApJ, 627, 53
Clavel, J., et al. 1990, MNRAS, 246, 668
Dietrich, M., Hamann, F., Shields, J. C., Constantin, A., Heidt, J., Jäger, K., Vestergaard, M., & Wagner, S. J. 2003, ApJ, 589, 722
Downes, D., Neri, R., Wiklind, T., Wilner, D. J., & Shaver, P. A. 1999, ApJ, 513, L1
Egami, E., Neugebauer, G., Soifer, B. T., Matthews, K., Ressler, M., Becklin, E. E., Murphy, T. W., & Dale, D. A. 2000, ApJ, 535, 561
Elvis, M., et al. 1994, ApJS, 95, 1
Ferland, G. J., Korista, K. T., Verner, D. A., Ferguson, J. W., Kingdon, J. B., & Verner, E. M. 1998, PASP, 110, 761
Glikman, E., Helfand, D. J., & White, R. L. 2006, ApJ, 640, 579
Hines, D. C., Krause, O., Rieke, G. H., Fan, X., Blaylock, M., & Neugebauer, G. 2006, ApJ, 641, L85
Hjorth, J., et al. 2002, ApJ, 572, L11
Huffman, D. R. 1977, Adv. Phys., 26, 129
Ibata, R. A., Lewis, G. F., Irwin, M. J., Lehár, J., & Totten, E. J. 1999, AJ, 118, 1922
Irwin, M. J., Ibata, R. A., Lewis, G. F., & Totten, E. J. 1998, ApJ, 505, 529
Iwamuro, F., Kimura, M., Eto, S., Maihara, T., Motohara, K., Yoshii, Y., & Doi, M. 2004, ApJ, 614, 69
Jakobsson, P., Hjorth, J., Burud, I., Letawe, G., Lidman, C., & Courbin, F. 2005, A&A, 431, 103
Jiang, L., et al. 2006, AJ, 132, 2127
Kaspi, S., et al. 1996, ApJ, 470, 336
Kawara, K., Murayama, T., Taniguchi, Y., & Arimoto, N. 1996, ApJ, 470, L85
Kobayashi, Y., Sato, S., Yamashita, T., Shiba, H, & Takami, H. 1993, ApJ, 404, 94
Kurk, J. D., et al. 2007, ApJ, 669, 32
Landt, H., Bentz, M. C., Ward, M. J., Elvis, M., Peterson, B. M., Korista, K. T., & Karovska, M. 2008, ApJS, 174, 282
Maoz, D., et al. 1991, ApJ, 367, 493
Matsuoka, Y., Kawara, K., & Oyabu, S. 2008, ApJ, 673, 62
Matsuoka, Y., Oyabu, S., Tsuzuki, Y., & Kawara, K. 2007, ApJ, 663, 781
Minezaki, T., Yoshii, Y., Kobayashi, Y., Enya, K., Suganuma, M., Tomita, H., Aoki, T., & Peterson, B. A. 2004, ApJ, 600, L35
Moshir, M., Kopman, G., & Conrow, T. A. O. 1992, IRAS Faint Source Survey, Explanatory Supplement, version 2 (Pasadena, CA: Infrared Processing and Analysis Center, Cal. Tech.)
Murakami, H., et al. 2007, PASJ, 59, 369
Nagao, T., Marconi, A., & Maiolino, R. 2006, A&A, 447, 157
Ohyama, Y., et al. 2007, PASJ, 59, 411
Onaka, T., et al. 2007, PASJ, 59, 401
Osterbrock, D. E. 1989, Astrophysics of Gaseous Nebulae and Active Galactic Nuclei (Mill Valley, CA: Univ. Science Books)
Oyabu, S., et al. 2001, A&A, 365, 409
Oyabu, S., et al. 2007, PASJ, 59, 497
Salpeter, E. E. 1977, ARA&A, 15, 267
Sanders, D. B., Phinney, E. S., Neugebauer, G., Soifer, B. T., & Matthews, K. 1989, ApJ, 347, 29
Soifer, B. T., et al. 2004, ApJS, 154, 151
Tsuzuki, Y., Kawara, K., Yoshii, Y., Oyabu, S., Tanabé, T., & Matsuoka, Y. 2006, ApJ, 650, 57
Weiß, A., Downes, D., Neri, R., Walter, F., Henkel, C., Wilner, D. J., Wagg, J., & Wiklind, T. 2007, A&A, 467, 955
Weingartner, J. C., & Draine, B. T. 2001, ApJ, 548, 296
Wills, B. J., Netzer, H., & Wills, D. 1985, ApJ, 288, 94
York, D. G., et al. 2000, AJ, 120, 1579
Yoshii, Y., Tsujimoto, T., & Kawara, K. 1998, ApJ, 507, L113